PREDICTION OF TIME TO FAILURE FOR OPTICAL FIBRES UNDER THERMO-MECANICAL STRESSES

R. El Abdi[1], R. Leite Pinto[2]
[1]Univ. Rennes- CNRS, Institut de Physique de Rennes. UMR 6251. F-35000 Rennes, France
[2]Entreprise Acom – Usines de Mortain, 50140 Mortain, France
Email: rochdi.el-abdi@univ-rennes.fr

Abstract - Considering measurement accuracies, different models used for the prediction of long-term static fatigue for optical fibres under stress were studied. Optical fibres were wound onto an alumina mandrel with various diameters and immersed in hot water at different temperatures.
The determination of model parameters was based on the fit of experimental data to model expressions relating time to failure, applied stress and environmental conditions.
It is shown that the differences in allowed stress predictions between models become quite close at short times. The time-to-failure depends on the applied stress applied but also and above all on the ageing temperature and the humidity level. Results from tested fibres indicate a clear strength reduction with increasing temperature or applied stress.

Keywords: Optical fibres, Lifetime measurement, Fatigue models, Fibres reliability.

1. Introduction

To characterize the mechanical reliability of optical fibres [1, 2], three techniques are used to give stress to the fibres have been introduced by IEC-60793-1-33, including, axial tension, two-point bending and uniform bending. Different with axial tension, which mainly describes the fibre condition in cables used for long distances, two-point bending and uniform bending mainly refer to the fibre stress condition that in access networks or in FTTH (Fiber To The Home). Along with the development of FTTH, many works focused on the lifetime or mechanical reliability of bend-insensitive fibres under small radius bending [3-6].

In this paper, a lifetime measurement system of uniform bending technique is introduced. Four models to estimate the time to failure were studied for different thermomechanical conditions for optical fibres used in telecommunication networks. Detailed influence factors like temperature, humidity and measurement dispersion are discussed here.

2. Optical Fibre Used

The used monomode fibre has two acrylate coatings (primary and outer coatings).

This fibre was manufactured using the Outside Vapor Deposition (OVD) process which produces a totally synthetic, ultra-pure fibre. It has high strength and low attenuation. Its dual acrylate layer (CPC6) coating provides excellent fibre protection. On the other hand, the operating temperature range was -60°C to +70 °C. A soft, primary coating has a low module of elasticity, adheres closely to the glass fibre and forms a stable interface. It protects the fragile glass fibre against micro-bending and attenuation. The outer coating protects the primary coating against mechanical damage and acts as a barrier to lateral forces. It has a high glass temperature and Young modulus and a good chemical resistance. The combined coating diameter is 245 μm ± 5μm, the clad diameter is 125 μm ± 1μm and the coating thickness is equal to 62.5 μm ± 2μm.

3. Test Bench Used

Optical fibre was wound onto an alumina mandrel of 2.8, 3, 3.2 or 3.4 mm in diameter (Fig. 1). The extremities were clamped in two oblique cuts simple clamping rings, made of elastomer-rubber, and mounted on the extremities of the alumina mandrels. This technique provides a useful length for 16 twisting tests.

Once the fibre was wound around the mandrel, it was placed between a transmitter and a light receiver. The light beam cannot reach the receiver and from then on, the time of fibre loading is triggered. When the fibre breaks, it falls. The light beam can reach the receiver and then the chronometer is stopped. The aging time is then recorded by a computing device.

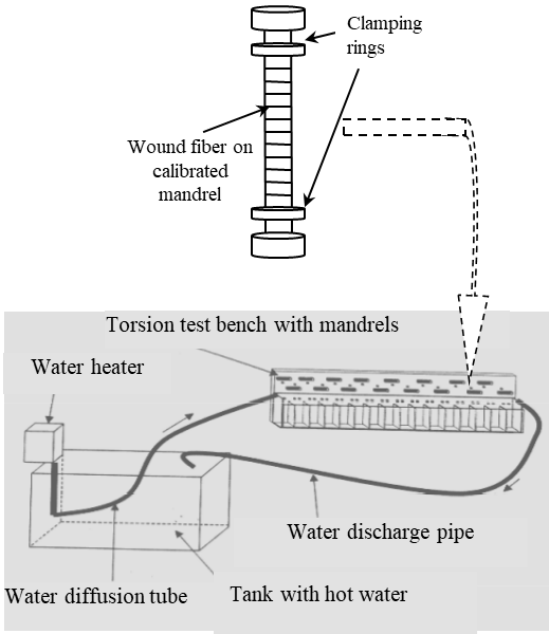

Figure 1: Mandrel sample with wound optical fibre and test bench with several samples

For fibre aging in hot water, we developed a water circulation system (Fig.1). The system comprises a 9 litre plastic tank in which is immersed a water heater with a resistance heater and a discharge pump. A water diffusion tube sends water at the desired temperature to the testing bench with mandrels. Thus, the fibres (wound around a mandrel) can be aged in water at different temperatures.

4. Theoretical Equations Used

The applied stress on the fibre depends on the mandrel diameter accordingly to the Mallinder and Proctor relation [7], as follows:

$$\sigma = E_0 . \varepsilon \left(1 + \frac{\alpha' . \varepsilon}{2}\right) \tag{1}$$

where σ is the applied stress (GPa); E_0 is the Young modulus (= 72 GPa for the silica); ε is the relative deformation of the fibre; $\alpha' = 0.75\,\alpha$ and α is the elastic constant of non-linearity (= 6).

The relative deformation of the fibre depends on the mandrel calibrated diameter, as follows:

$$\varepsilon = \frac{d_{glass}}{\phi + d_{fiber}} \tag{2}$$

ϕ is the mandrel diameter (in µm); d_{glace} is the glass fibre diameter (= 125 µm); d_{fiber} is the fibre diameter (= 250 µm), including the layer polymer coating. This leads, in the case of a usual fibre, to the corresponding stresses of 3.22 GPa for the calibrated diameter mandrel of 2.8 mm.

One can note that a wound fibre was subjected to compressive stresses on its internal part (fibre surface close to the curvature center) and a tensile stress on its external part (fibre surface furthest away from the curvature center).

It's not easy to predict the fibre lifetime from accelerated testing data because is certainly more difficult to estimate the confidence interval than the expected fibre lifetime. Therefore, different models were used and didn't lead to exactly to the same predictions.

For silica materials containing macroscopic cracks, chemical attacks such as the humidity lead to bond failure at the crack tip and then to crack propagation. Four models were commonly used and depend on the applied stress, on stress intensity factor, on the crack shape and on environmental conditions (temperature and humidity dependence). The following models giving the lifetime prediction will be used [8]:

- Model 1:

$$t_f = \frac{1}{\sigma^2} . \frac{2K_{IC}{}^2}{A_1{}^2 Y^2 (n_1 - 2)} . \left(\frac{\sigma}{S}\right)^{2-n_1} \tag{3}$$

- Model 2:

$$t_f = \frac{1}{\sigma^2} . \frac{2K_{IC}{}^2}{A_2{}^2 Y^2 n_2} . e^{\left(-n_2 . \left(\sigma/S\right)\right)} . \left(\frac{\sigma}{S} + \frac{1}{n_2}\right) \tag{4}$$

- Model 3:

$$t_f = \frac{1}{\sigma^2} . \frac{2K_{IC}{}^2}{A_3{}^2 Y^2 n_3} . e^{\left(-n_3 . \left(\sigma/S\right)^2\right)} \tag{5}$$

- Model 4:

$$t_f = \frac{1}{\sigma^2} . \frac{2K_{IC}{}^2}{A_4{}^2 Y^2 n_4} . e^{\left(-n_4 . \left(\sigma/S\right)\right)} \tag{6}$$

where t_f is the failure time, Y is a dimensionless factor of order unity dependent on the crack geometry, K_{IC} is the critical stress intensity factor for fast fracture, σ is the applied stress. A_i parameters (i=1 through 4) are pre-factors temperature and humidity dependent, S is the initial inert strength of the material (strength in the absence of fatigue) and n_1 is the stress corrosion parameter.

If a representative stress σ_0 gives a time to failure t_0, then we constrain the models to have the same t_f and $dt_f / d\sigma$ at $\sigma = \sigma_0$. If the inert strength S for the accelerated fatigue data is defined as So, then it may be shown that:

$$n_2 = \frac{S_o (n_1 - 1)}{\sigma_o} \tag{7}$$

$$n_3 = \frac{S_o{}^2 (n_1 - 2)}{2 . \sigma_o{}^2} \tag{8}$$

$$n_4 = \frac{S_o\ (n_1 - 2)}{\sigma_o} \qquad (9)$$

Equation (3) can have a linearized form:

$$Ln(t_f) = -n_1 . Ln(\sigma) + \alpha_1 \qquad (10)$$

Table 1 gives time to failures for different temperatures and different applied stresses (mandrel diameters ϕ).

Table 1. Time to failure for different stresses (mandrel diameters) and water temperatures

	2.59 GPa ϕ=3.4 mm	**2.75 GPa ϕ=3.2 mm**	**2.93 GPa ϕ=3.0 mm**	**3.13 GPa ϕ=2.8 mm**
20°C	162h 14min 13s	26h 22min 30s	5h 20min 41s	1h 28min 13s
30°C	46h 2min 9s	10h 22min 30s	1h 54min 15s	46min 26s
40°C	17h 24min 29s	2h 48min 32s	40 min 20s	11min 42s
50°C	9h 15min 34s	2h 11min 17s	20min 25s	10min 46s
60°C	5h 27min 11s	1h 4min 8s	13min 40s	6min 19s
70°C	1h 5min 1s	26min 11s	8min 4s	2min 5s

The temperature and the mandrel diameter have a significant influence on time to failure. Indeed, for the same temperature, the time to failure can be divided by 100 (for 20°C, time to failure decreases from 162h 14min for ϕ = 3.4mm to 1h28min for ϕ= 2.8mm).

On the other hand, for the same stress (same winding diameter), the time to failure can be divided by 150 (for ϕ = 3.4mm, time to failure decreases from 162h 14min for 20°C to 1h5min for 70°C).

The classical Weibull plots showing the logarithm function of the cumulative failure probability *Ln{[-1/L]. Ln(1-F)}*, where *F* (in %) represents the cumulative probability to failure for each stress to fracture σ (in GPa), related to the time to failure has allowed to find the statistical parameters, namely: the medium time value t_{med}, the median stress $\sigma_{(50\%)}$, corresponding to a probability to fracture *F*=50 % .

Fig. 2 gives Weibull curves for fibres wounded onto an alumina mandrel of 2.8, 3, 3.2 and 3.4 mm in diameter aged in water at 20°C.

For each mandarin diameter, one can calculate the applied stress using Eqs (1) and (2) and obtain the logarithm function of the time to failure *Ln* (t_f, in h) related to the logarithm of the stress *Ln* (σ, in GPa) (Fig. 3). A linear interpolation gives the stress corrosion parameter value n_1 using Eq. (10).

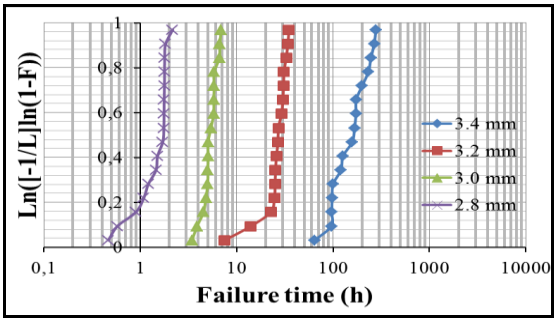

Figure 2: Weibull plots for different mandrel diameters for aging in water at 20°C

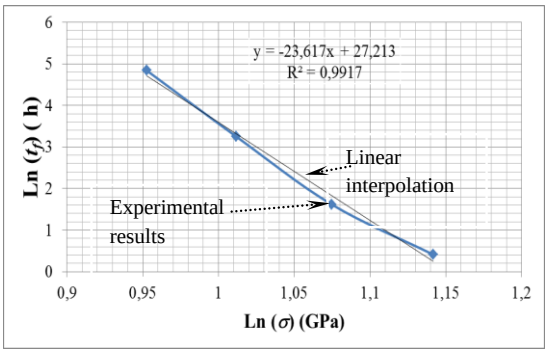

Figure 3: Time to failure versus applied stress (aging in water at 20°C)

For each temperature, the stress corrosion parameter n_1 was obtained and then the other parameters n_i (i=2, 4) that define models (2, 3 and 4), when one uses Eqs. 7- 9 with an inert stress *So* equal to 10 GPa. On the other hand Eqs. 4 to 6 were used to find the best n_i (i=2, 4) parameters which lead to obtain a good value of measured time to failure. Table 2 gives for different temperatures, the n_i (i=2, 4) parameters deduced from n_1 values (Experimental values) and those deduced from the use of models (Model value). The general trend was that the parameters obtained from the models were close to that obtained from experimental results.

Table 2. n_i parameters for different temperatures and models (1 to 4) (S_0 = 120 GPa)

	20°C		**30°C**		**40°C**		**50°C**		**60°C**		**70°C**	
	Exp.	Model	Exp.	Model	Exp.	Model	Exp.	Model	Exp.	Model	Exp.	Model
n_1	23.6±6		23.1±6		21.5±6		21.7±6		20.4±6		18.6±5	
n_2	77±6	82±12	75±6	83±13	70±6	73±10	71±6	70±15	66±5	61±11	60±5	60±2
n_3	126±20	136±24	123±20	141±25	114±19	118±19	115±19	114±29	107±17	98±21	97±16	99±1
n_4	74±6	79±12	72±6	79±13	66±5	69±10	67±5	66±15	63±5	58±11	57±5	57±1

Thus, using the four models, we can calculate the time to failure when a fibre was submitted to another stress than those used during our tests. For example, for a stress equal to 0.216 GPa (ϕ= 4cm), the four models lead to similar time to failure (Table 3).

Table 3. Time to failure for different models (σ = 0.216 GPa)

	Model 1	**Model 2**	**Model 3**	**Model 4**
20°C	3.15 months	3 months	2.5 months	3 months
30°C	35 days	34 days	1 month	36 days
40°C	9.25 days	8 days	7 days	8 days
50°C	7 days	5 days	1 day	5 days
60°C	3 days	3 days	40 hours	2 days
70°C	1 day	18 hours	17 hours	20 hours

5. Conclusions

It should be noted for relatively short times to failure such as those obtained for optical fibres tested in hot water, the four models lead to a good approximation of the time to failure. For fairly long service lives, such for as fibres subjected to low stresses and aged in air at ambient temperature, the time to failure exceeds several years and the four models can lead to different estimations.

In this case, the uncertainty in the crack growth model can't be ignored in making reliability predictions for optical fibre under stress. The statistical uncertainty is significant also, but is usually smaller than the model uncertainty. The differences in allowed stress predictions between models become quite large at long times [8].

On one hand, the microcracks in each fibre are different and their number varies from one fibre to another.

Furthermore, and during long-term ageing, damage phenomena must be taken into account and are not described by the models. That needs a better understanding of crack growth and the chemical environment action on the fibre aging.

Acknowledgements

The authors express their gratitude to Entreprise Acome (Usines de Mortain – 50140 Mortain, France) and to AFL Specialty Fiber (Verrillon, Inc – North Grafton 01536, MA- USA) for technical assistance and for material support.

References

[1] Griffioen, W.: Evaluation of optical fiber lifetime models based on the power law. Optical Engineering 33(2), 488- 497(1994).

[2] IEC TR 62048: Optical fibres -Reliability-Power law theory. International Electronics Commission (2014).

[3] Shang, H., Hou, L., Chou, G., Hsieh, R.: Lifetime predictions of bend optimized GGP single mode fiber for FTTH requirement, Proceedings of the 57th IWCS (2008).

[4] Mazzarese, D., Weimann, P., Norris, R., Konstadinidis, K.: Reliability considerations for next-generation bendoptimized fibers. Proceedings of the 57th IWCS (2008).

[5] Griffioen, W., Greven, W., Jonker, J., Zandberg, S., Kuyt, G., Overton, B.: Reliability of bend insensitive fibers. Proceedings of the 57th IWCS (2008).

[6] Zhang, L., Li, J., Yan, C., Liu, Li.: Static n value and lifetime measurement of bend-insensitive optical fibres by uniform bending method. International Wire & Cable Symposium. Proceeding of the 66th IWCS Conference. pp. 189-193 (2017).

[7] Mallinder, F.P. and Proctor, B.A.: Elastic constants of fused silica as a function of large tensile strain. Phys. Chem. Glass., Vol. 5, 91-103 (1964).

[8] Bubel, G.M. and Matthewson, M.J.: Optical fiber reliability implications of uncertainty in the fatigue crack growth model. Optical Engineering, Vol. 30, N°6, 737-745 (1991).